Journal of Computational and Applied Mathematics 325 (2017) 56–73

Contents lists available at ScienceDirect

Journal of Computational and Applied Mathematics

journal homepage: www.elsevier.com/locate/cam

Spectral variational integrators for semi-discrete Hamiltonian wave equations

Yiqun Li [a,*], Boying Wu [a], Melvin Leok [b]

[a] Department of Mathematics, Harbin Institute of Technology, Harbin 150001, PR China

[b] Department of Mathematics, University of California at San Diego, La Jolla, CA 92093, USA

ARTICLE INFO

Article history:
Received 8 February 2016
Received in revised form 21 April 2017

Keywords:
Hamiltonian PDEs
Spectral variational integrator
Semi-discrete
Symmetric difference

ABSTRACT

In this paper, we present a highly accurate Hamiltonian structure-preserving numerical method for simulating Hamiltonian wave equations. This method is obtained by applying spectral variational integrators (SVI) to the system of Hamiltonian ODEs which are derived from the spatial semi-discretization of the Hamiltonian PDE. The spatial variable is discretized by using high-order symmetric finite-differences. An efficient implementation of SVI for high-dimensional systems of ODEs is presented.

1. Introduction

During the past decade, there have been many attempts to derive geometric structure-preserving numerical methods for Hamiltonian PDEs [1–3]. Researchers have tried to extend the ideas in the geometric integration of ODE systems to construct numerical schemes for some specific PDEs, so as to preserve as many invariants of the systems as possible. These approaches have mainly focused on multisymplectic variational integrators [4], multisymplectic reformulation of the Hamiltonian PDEs [5] or using some geometric structure-preserving ODE solvers, such as Gauss collocation, discrete gradients and the average vector field methods, applied to the invariant-preserving semi-discrete ODEs [6]. Without loss of generality, we consider the Hamiltonian wave equations described in [4],

$$\frac{\partial^2 u}{\partial t^2} - \Delta u - V'(u) = 0, \quad u \in \Gamma(\pi_{XY}), \tag{1}$$

where $\pi_{XY} : Y \to X$ is a fiber bundle over the oriented space–time manifold X, V is a real valued C^∞ function, and $u : X \to Y$ is a section of π_{XY}, and $j^1(u)$ is its first jet extension. For a more in-depth discussion of multisymplectic geometry, the reader is referred to Gotay [7].

By drawing upon variational formulations of field theories and multisymplectic geometry, Marsden et al. [4] introduced the abstract multisymplectic formulation of Hamiltonian PDEs and constructed multisymplectic variational integrators based on triangles and rectangles (see Fig. 1). The main advantage of the covariant multisymplectic perspective in the discretization of Hamiltonian PDEs is that it allows one to consider discretizations of the configuration bundle that are not simply global tensor products of spatial and temporal discretizations, which is what one would obtain otherwise by applying a symplectic integrator to the semi-discretization of the Hamiltonian PDE. This flexibility is exploited in Lew et al. [8] to obtain multisymplectic integrators in which the different spatial elements are time-marched using different time-steps.

* Corresponding author.
E-mail addresses: liyiqun_hit@163.com (Y. Li), mathwby@hit.edu.cn (B. Wu), mleok@math.ucsd.edu (M. Leok).

http://dx.doi.org/10.1016/j.cam.2017.04.043
0377-0427/

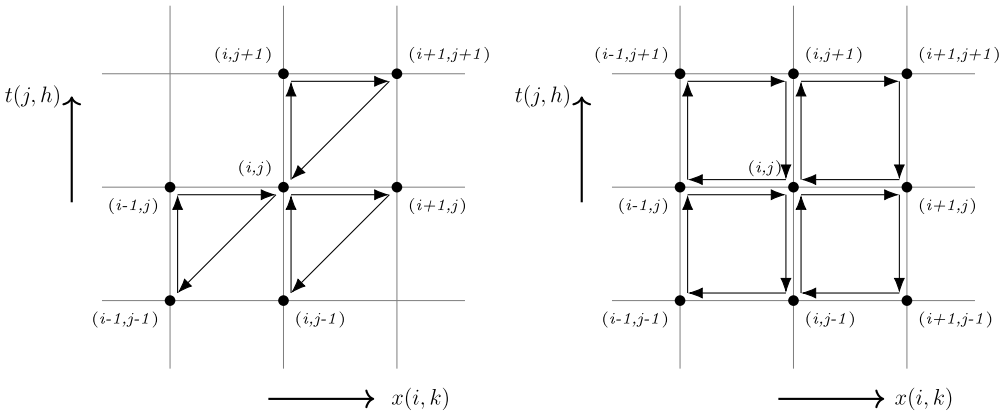

Fig. 1. On the left, the method based on a regular triangular mesh; on the right, the method based on a regular rectangular mesh.

In analogy to variational integrators for ODEs, there are two main steps for constructing multisymplectic variational integrators. One is to choose a finite-dimensional function space to approximate sections $u : \mathcal{X} \to Y$ of the configuration bundle Y. The other is to choose a quadrature method to approximate the action integral $\mathfrak{S} = \int_{\mathcal{X}} L(j^1\phi)$.

An alternative approach to the construction of multisymplectic integrators was introduced by Bridges and Reich [9], and is based on a description of a Hamiltonian PDE in terms of multiple skew-symmetric matrices, which is the notion of multisymplectic geometry introduced in Bridges [5]. In this framework, the $(1 + 1)$-dimensional nonlinear wave equation (1) can be expressed as

$$v_t + w_x - V'(u) = 0, \quad v = u_t, \ -w = u_x,$$

which can be written in multisymplectic form

$$\begin{bmatrix} 0 & -1 & 0 \\ 1 & 0 & 0 \\ 0 & 0 & 0 \end{bmatrix} \begin{bmatrix} u_t \\ v_t \\ w_t \end{bmatrix} + \begin{bmatrix} 0 & 0 & -1 \\ 0 & 0 & 0 \\ 1 & 0 & 0 \end{bmatrix} \begin{bmatrix} u_x \\ v_x \\ w_x \end{bmatrix} = \begin{bmatrix} -V'(u) \\ v \\ -w \end{bmatrix},$$

or more compactly as

$$MZ_t + KZ_x = \nabla_Z H(Z).$$

Many high-order multisymplectic integrators [10,11] have been constructed and analyzed based on both semi-discretizations and full-discretizations using this formulation.

Remark 1.1. Multisymplectic field theories expressed in terms of a multisymplectic $(n + 2)$-differential form in the sense proposed by Marsden reduce to the Bridges' formulation of multisymplectic field theories for a suitable choice of skew-symmetric matrices for each of the spatial and temporal components. However, the converse is not true. This is because the skew-symmetric matrices in the Bridges formulation have to satisfy an integrability condition for them to be expressible as a single multisymplectic $(n + 2)$-differential form. This is analogous to the fact that every n-order differential equation can be expressed as a system of n first-order differential equations, but not every system of n first-order differential equations can be expressed as a single n-order differential equation.

In this paper, we focus on solving the large system of Hamiltonian ODEs obtained by semi-discretization of the Hamiltonian PDE using spectral variational integrators (SVI), which fall within the framework of generalized Galerkin variational integrators that have been discussed in [12–15]. Hall and Leok [12] provide a systematic introduction to spectral variational integrators. In addition to the spectral accuracy, the SVI is symplectic, momentum-preserving and exhibits excellent energy behavior. We will also see that the stability and computational efficiency of spectral variational integrators are both favorable when compared with some symplectic Runge–Kutta methods [16], which makes SVIs an excellent choice to deal with the Hamiltonian ODEs that arise from the semi-discretization of Hamiltonian PDEs. As to the Hamiltonian preserving semi-discretization of the spatial variables, one may choose symmetric finite-difference [17], spectral discretizations or the rescaled Fourier discretization [18]. No matter which discretization we choose, the basic goal is to conserve discrete counterparts of the continuous invariants.

The outline of this paper is as follows. In Section 2, we introduce the Hamiltonian preserving semi-discretization of the given Hamiltonian PDE. In Section 3, we briefly review the construction of SVIs and give an efficient implementation of SVIs for high-dimensional systems of ODEs. In Section 4, a simple error estimate is given. Numerical examples together with some comparisons are then presented in Section 5. Here, we consider the linear wave equation and the breather solution of sine-Gordon equations. In Section 6, we draw some conclusions and provide possible future directions.

Table 1
Coefficients of symmetric differences.

Order	α_{i-4}	α_{i-3}	α_{i-2}	α_{i-1}	α_i	α_{i+1}	α_{i+2}	α_{i+3}	α_{i+4}
2				1	-2	1			
4			$-\frac{1}{12}$	$\frac{4}{3}$	$-\frac{5}{2}$	$\frac{4}{3}$	$-\frac{1}{12}$		
6		$\frac{1}{90}$	$-\frac{3}{20}$	$\frac{3}{2}$	$-\frac{49}{18}$	$\frac{3}{2}$	$-\frac{3}{20}$	$\frac{1}{90}$	
8	$-\frac{1}{560}$	$\frac{8}{315}$	$-\frac{1}{5}$	$\frac{8}{5}$	$-\frac{205}{72}$	$\frac{8}{5}$	$-\frac{1}{5}$	$\frac{8}{315}$	$-\frac{1}{560}$

2. Semi-discretization of the Hamiltonian wave equation

The basic idea of our approach is that we first discretize the spatial dimensions in a highly accurate way, so that the resulting semi-discrete problem is a Hamiltonian system of ODEs to which Galerkin spectral variational integrators can be applied directly. Without loss of generality, we consider the one-dimensional wave equation with periodic boundary conditions which are given as,

$$\begin{cases} \dfrac{\partial^2 u(x,t)}{\partial t^2} = \dfrac{\partial^2 u(x,t)}{\partial x^2} + V'(u(x,t)), \quad (x,t) \in (-R,R) \times (0,\infty), \\ u(x,0) = \psi_0(x), \qquad u_t(x,0) = \psi_1(x), \\ u(-R,t) = u(R,t). \end{cases} \tag{2}$$

2.1. Symmetric finite-difference approach

There are several ways we can use to approximate the second-order spatial derivative, such as, finite-differences, finite elements, or Fourier–Galerkin, all of which yield a set of Hamiltonian ODEs of the following form,

$$\frac{d^2\mathbf{u}}{dt^2} = D\mathbf{u} + F(t,\mathbf{u}), \quad 0 < t \le \infty, \tag{3}$$

where

$$\mathbf{u}(t) = (u_0(t), \ldots, u_N(t))^T \quad \text{with } u_i(t) \approx u(x_i,t),$$
$$F(t,\mathbf{u}) = (V'(u_0), \ldots, V'(u_N))^T.$$

A semi-discretization on the spatial variable by using second-order symmetric differences is given by,

$$\frac{d^2 u_i}{dt^2} = \frac{u_{i+1} - 2u_i + u_{i-1}}{\Delta x^2} + V'(u_i), \quad 0 < t \le \infty, \tag{4}$$

which lead to a system of ODEs of the form (3) with differentiation matrix

$$D = \frac{1}{\Delta x^2} \begin{pmatrix} -2 & 1 & & & 1 \\ 1 & -2 & 1 & & \\ & \ddots & \ddots & \ddots & \\ & & 1 & -2 & 1 \\ 1 & & & 1 & -2 \end{pmatrix}_{(N-1)\times(N-1)}. \tag{5}$$

For higher-order symmetric differences methods

$$\frac{\partial^2 u(x_i,t)}{\partial x^2} \approx \frac{1}{\Delta x^2} \sum_{j=-k}^{k} \alpha_{i+j} u_{i+j}, \tag{6}$$

which are even-order generalizations of the central difference scheme, we can refer to Table 1. It should be mentioned that in order to use the $p = 2k$ order schemes for boundary-value problems, we need k boundary conditions. For a more systematic introduction of high-order finite-difference scheme, readers may refer to [19,17].

Remark 2.1. Since the eigenvalue λ of (5) is between $-\frac{4}{\Delta x^2}$ and 0, the semi-discrete system (3) becomes extremely stiff when we choose a small Δx. But numerically we will observe that spectral variational integrators are still effective for this stiff high-dimensional system of ODEs. Refer to Fig. 2 for the eigenvalues of D which we will use later in the numerical simulations.

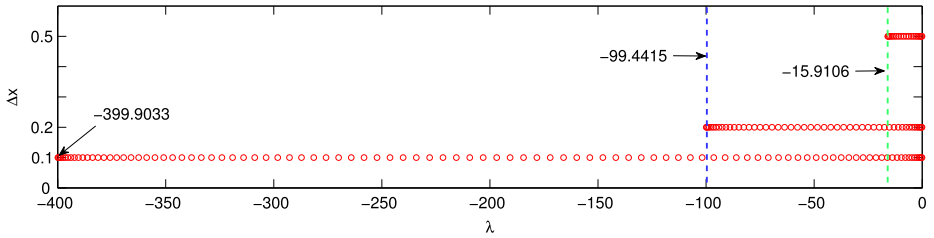

Fig. 2. Eigenvalues of the second-order symmetric finite-difference matrix with different spatial discretizations in the spatial domain $[-5, 5]$.

Theorem 2.1. *Suppose V is continuously differentiable and $\mathbf{u}(t) = (u_0(t), \ldots, u_N(t))^T$ is the solution of (3), then the Hamiltonian that generates (3) is given by*

$$H(\mathbf{u}, \dot{\mathbf{u}}) = \Delta x \left[\frac{1}{2}\dot{\mathbf{u}}^T\dot{\mathbf{u}} + \frac{1}{2}\mathbf{u}^T D\mathbf{u} + \sum_{i=0}^{N} V(u_i) \right], \tag{7}$$

and in particular, the Hamiltonian is a constant of motion.

Proof. It is easy to check that the Hamilton's equation associated with the Hamiltonian are given by (3), and to verify that $\frac{dH(t)}{dt} = 0$ by using the fact that D is symmetric. □

A more natural way to convert the infinite-dimensional nonlinear wave equation to finite-dimensional Hamiltonian systems is to discretize the continuous Lagrangian of the wave equation directly. We will see that this implementation can give us systems of Hamiltonian ODEs with arbitrarily high accuracy. As a simple example, we can replace the Lagrangian of (2)

$$L(t, x, u, u_t, u_x) = \frac{1}{2}\left[\left(\frac{\partial u}{\partial t}\right)^2 - \left(\frac{\partial u}{\partial x}\right)^2 \right] + V(u), \tag{8}$$

by the following semi-discrete analogue,

$$L(t, \mathbf{u}, \mathbf{u}_t) = \sum_{i=0}^{N-1} \left\{ \frac{1}{2}\left[\left(\frac{\partial u_i}{\partial t}\right)^2 - \left(\frac{u_{i+1} - u_i}{h}\right)^2 \right] + V(u_i) \right\}.$$

Then, the Euler–Lagrange equations

$$\frac{d}{dt}\frac{\partial L}{\partial \dot{u}_i} - \frac{\partial L}{\partial u_i} = 0,$$

lead to the second-order finite-difference scheme,

$$\ddot{u}_i - \frac{1}{h^2}(u_{i-1} - 2u_i + u_{i+1}) + V'(u_i) = 0, \quad i = 1, \ldots, N-1$$

which is the same as (4). The Hamilton's canonical equations can also be obtained by discretizing the spatial variables of the continuous Hamiltonian,

$$H(t, \mathbf{u}, \mathbf{u}_t) = \sum_{i=0}^{N-1} \left\{ \frac{1}{2}\left[\left(\frac{\partial u_i}{\partial t}\right)^2 + \left(\frac{u_{i+1} - u_i}{h}\right)^2 \right] + V(u_i) \right\}.$$

Then, Hamilton's canonical equations are given as,

$$\ddot{u}_i = -\frac{\partial H}{\partial u_i}, \qquad \dot{u}_i = \frac{\partial H}{\partial \dot{u}_i},$$

or more compactly as

$$\frac{d\mathcal{Z}}{dt} = J^{-1}\Delta H(\mathcal{Z}),$$

where $\mathcal{Z} = (\mathbf{u}, \dot{\mathbf{u}})$ and J is the symplectic matrix,

$$J = \begin{pmatrix} 0_{N-1} & I_{N-1} \\ -I_{N-1} & 0_{N-1} \end{pmatrix}.$$

2.2. Spectral collocation approach

We can also use a spectral collocation method to discretize the spatial derivative which led to Hamiltonian ODEs with higher-order spatial approximation. Combined with the SVI for solving the resultant system of Hamiltonian ODEs, the numerical methods can obtain overall (space–time) spectral accuracy.

We discretize (8) in space by using the spectral collocation method, which led to the following discrete (spatial) Lagrangian

$$L(t, \mathbf{u}, \mathbf{u}_t) = \sum_{i=0}^{N} \left\{ \frac{1}{2} \left[\left(\frac{\partial u_i}{\partial t} \right)^2 - \left(\sum_{k=0}^{N} D_{ik}^{(1)} u_k \right)^2 \right] + V(u_i) \right\},$$

where $D_{ik}^{(1)}$ are the entries of the first-order spectral differentiation matrix $D^{(1)}$ in the spatial domain $[-R, R]$ and the construction of the spectral differentiation matrix for arbitrary order can be found in [20]. Then the Euler–Lagrange equations led to the corresponding ODEs,

$$\ddot{\mathbf{u}} = A\mathbf{u} + V'(\mathbf{u}), \tag{9}$$

where

$$A = \begin{pmatrix} (a_1, a_1) & (a_1, a_2) & \dots & (a_1, a_{N+1}) \\ (a_2, a_1) & (a_2, a_2) & \dots & (a_2, a_{N+1}) \\ \vdots & \vdots & \ddots & \vdots \\ (a_{N+1}, a_1) & (a_{N+1}, a_2) & \dots & (a_{N+1}, a_{N+1}) \end{pmatrix}$$

and (a_i, a_j) is the inner product of the ith and jth columns of the matrix $D^{(1)}$. We can see that matrix A is automatically symmetric. The derivative of u with respect to x may be approximated by any appropriate differentiation matrix, such as Legendre, Hermite and sinc differentiation matrix [18]. We can also use a Fourier–Galerkin approximation [21,6]. It should be pointed out that the spectral variational integrators may not be stable for every system of Hamiltonian ODEs constructed in this way, but we will see from the numerical experiments that SVIs are effective for many of the resulting stiff systems which cannot otherwise be solved by many conventional ODE solvers.

3. Galerkin spectral variational integrators

We briefly recall the construction of spectral variational integrators, which falls within the framework of generalized Galerkin variational integrators that were discussed in [12,13,15,22]. We will introduce an efficient implementation for high-dimensional Hamiltonian systems, which are suitable for semi-discrete systems of Hamiltonian ODEs (9).

3.1. A brief introduction to discrete mechanics and variational integrators

Galerkin variational integrators fall within the general framework of discrete mechanics and variational integrators. We provide a brief introduction of discrete Lagrangian mechanics and variational integrators, and we refer the reader to [15] for a more comprehensive introduction. Discrete mechanics is based on a discrete analogue of Hamilton's principle,

$$\delta \mathfrak{S}_d = 0,$$

where $\mathfrak{S}_d : U^{M+1} \to \mathbb{R}$ is the discrete action sum defined as

$$\mathfrak{S}_d(\mathbf{u}_0, \mathbf{u}_1, \dots, \mathbf{u}_M) = \sum_{k=0}^{M-1} L_d(\mathbf{u}_k, \mathbf{u}_{k+1}) \approx \int_0^T L(\mathbf{u}, \dot{\mathbf{u}}) dt.$$

Let U denote the configuration manifold, $\mathbf{u}$ is a point on the configuration manifold, and $\mathbf{u}(t)$ is a curve on the configuration manifold. The discrete (time) Lagrangian, $L_d : U \times U \to \mathbb{R}$, is then an approximation of the exact discrete Lagrangian,

$$L_d^E(\mathbf{u}_k, \mathbf{u}_{k+1}) = \int_{t_k}^{t_{k+1}} L(\mathbf{u}_{k,k+1}(t), \dot{\mathbf{u}}_{k,k+1}(t)) dt, \tag{10}$$

where $\mathbf{u}_{k,k+1}(t)$ satisfies the Euler–Lagrange boundary-value problem, i.e., $\mathbf{u}_{k,k+1}(t_k) = \mathbf{u}_k$, $\mathbf{u}_{k,k+1}(t_{k+1}) = \mathbf{u}_{k+1}$ and $\mathbf{u}_{k,k+1}$ satisfies the Euler–Lagrange equation in the time interval $[t_k, t_{k+1}]$. Alternatively, for a fixed time-step h, one can characterize the exact discrete Lagrangian variationally as follows,

$$L_d^E(\mathbf{u}_k, \mathbf{u}_{k+1}; h) = \underset{\substack{\mathbf{u} \in C^2([kh,(k+1)h], U) \\ \mathbf{u}(kh) = \mathbf{u}_k, \mathbf{u}((k+1)h) = \mathbf{u}_{k+1}}}{\operatorname{ext}} \int_{t_k}^{t_{k+1}} L(\mathbf{u}(t), \dot{\mathbf{u}}(t)) dt. \tag{11}$$

Taking variations of the discrete action sum yield the discrete Euler–Lagrange (DEL) equations,

$$D_2L_d(\mathbf{u}_{k-1}, \mathbf{u}_k) + D_1L_d(\mathbf{u}_k, \mathbf{u}_{k+1}) = 0, \quad k = 1, \ldots, M-1 \tag{12}$$

which defines the discrete Lagrangian map $F_{L_d} : U \times U \to U \times U$, which is given by,

$$F_{L_d} : (\mathbf{u}_{k-1}, \mathbf{u}_k) \to (\mathbf{u}_k, \mathbf{u}_{k+1}).$$

This is equivalent to the implicit discrete Euler–Lagrange (IDEL) equations,

$$\mathbf{p}_k = -D_1L_d(\mathbf{u}_k, \mathbf{u}_{k+1}), \qquad \mathbf{p}_{k+1} = D_2L_d(\mathbf{u}_k, \mathbf{u}_{k+1}), \tag{13}$$

which implicitly defines the discrete Hamiltonian map $\tilde{F}_{L_d} : T^*U \to T^*U$, which is given by,

$$\tilde{F}_{L_d} : (\mathbf{u}_k, \mathbf{p}_k) \to (\mathbf{u}_{k+1}, \mathbf{p}_{k+1}).$$

Here, D_1, D_2 denote partial derivatives with respect to the first and second variables, respectively. Numerical integration schemes described by the discrete Lagrangian and Hamiltonian maps are referred to as variational integrators, which are automatically symplectic, momentum preserving and exhibit excellent long-time energy behavior. By introducing the discrete Legendre transforms [15], $\mathbb{F}^{\pm}L_d : U \times U \to T^*U$,

$$\mathbb{F}^+L_d : (\mathbf{u}_k, \mathbf{u}_{k+1}) \to (\mathbf{u}_{k+1}, \mathbf{p}_{k+1}) = (\mathbf{u}_{k+1}, D_2L_d(\mathbf{u}_k, \mathbf{u}_{k+1})),$$
$$\mathbb{F}^-L_d : (\mathbf{u}_k, \mathbf{u}_{k+1}) \to (\mathbf{u}_k, \mathbf{p}_k) = (\mathbf{u}_k, -D_1L_d(\mathbf{u}_k, \mathbf{u}_{k+1}))$$

the relationship between the discrete Hamiltonian map and discrete Lagrangian map can be illustrated by the following commutative diagram,

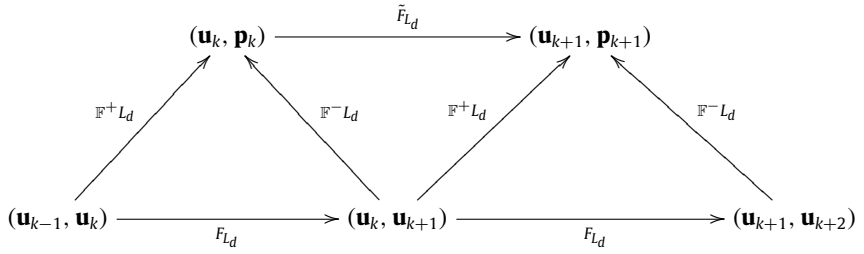

From the above diagram, it can be seen that $\tilde{F}_{L_d} : (\mathbf{u}_k, \mathbf{p}_k) \to (\mathbf{u}_{k+1}, \mathbf{p}_{k+1}) = \mathbb{F}^+L_d\left(\left(\mathbb{F}^-L_d\right)^{-1}(\mathbf{u}_k, \mathbf{p}_k)\right)$ and the following three definitions of the discrete Hamiltonian map are equivalent (Corollary 1.5.3 of [15]),

$$\tilde{F}_{L_d} = \mathbb{F}^+L_d \circ \left(\mathbb{F}^-L_d\right)^{-1},$$
$$\tilde{F}_{L_d} = \mathbb{F}^+L_d \circ F_{L_d} \circ \left(\mathbb{F}^+L_d\right)^{-1},$$
$$\tilde{F}_{L_d} = \mathbb{F}^-L_d \circ F_{L_d} \circ \left(\mathbb{F}^-L_d\right)^{-1}.$$

To approximate the integral in equation (11), one should first choose an interpolation function on the interval $[kh, (k+1)h]$ passing through $\mathbf{u}_k, \mathbf{u}_{k+1}$ to approximate $\mathbf{u}(t)$, then a quadrature formula can be applied to the integral of the Lagrangian evaluated along the chosen interpolation function. The following theorem states that the accuracy of the discrete Hamiltonian map is determined by the accuracy of the approximation of Eq. (11).

Theorem 3.1 (*Variational Error Analysis [15]*)**.** *Given a regular Lagrangian L and corresponding Hamiltonian H, the following are equivalent for a discrete Lagrangian L_d:*

(1) *the discrete Hamiltonian map for L_d is of order r,*

(2) *the discrete Legendre transforms of L_d is of order r,*

(3) *L_d approximate the exact discrete Lagrangian L_d^E with order r.*

3.2. Generalized Galerkin variational integrators

The motivating idea behind Galerkin variational integrators is to approximate the numerically non-computable exact discrete Lagrangian L_d^E with a highly-accurate computable discrete Lagrangian L_d. Specifically, for a given Lagrangian $L : TU \to \mathbb{R}$, generalized Galerkin variational integrators are constructed by the following steps:

Algorithm 1 Construction of Galerkin variational integrators

1: Choose an interpolation function space $\mathcal{C}^s([kh, (k+1)h], U)$ that is parameterized by $s+1$ points ($s-1$ internal points and 2 boundary points) with a set of basis functions $\{\phi_\nu(t)\}_{\nu=0}^s$ to approximate $\mathbf{u}$,

$$\mathbf{u}(t) = \sum_{\nu=0}^{s} \mathbf{u}^\nu \phi_\nu(t).$$

2: Choose a numerical quadrature rule

$$\int_a^b f(x)dx \approx \sum_{n=1}^{m} w_n f(\tau_n), \quad \tau_n \in [a, b],$$

where w_n are the quadrature weights and τ_n are the quadrature points.

3: Approximate the discrete action $\mathfrak{S}^s : \mathcal{C}^s([kh, (k+1)h], U) \to \mathbb{R}$ on the interval $[kh, (k+1)h]$ for a fixed time-step h,

$$\begin{aligned}\mathfrak{S}^s_{[kh,(k+1)h]}(\{\mathbf{u}_k^\nu\}_{\nu=0}^s) &= \sum_{n=1}^{m} w_n L\left(\sum_{\nu=0}^{s} \mathbf{u}_k^\nu \phi_\nu(\tau_n), \sum_{\nu=0}^{s} \mathbf{u}_k^\nu \dot{\phi}_\nu(\tau_n)\right)\\ &\approx \int_{kh}^{(k+1)h} L\left(\sum_{\nu=0}^{s} \mathbf{u}_k^\nu \phi_\nu(t), \sum_{\nu=0}^{s} \mathbf{u}_k^\nu \dot{\phi}_\nu(t)\right) dt.\end{aligned}$$

4: Construct the Galerkin discrete Lagrangian as

$$L_d(\mathbf{u}_k, \mathbf{u}_{k+1}; h) = \operatorname*{ext}_{\substack{\mathbf{u}\in\mathcal{C}^s([kh,(k+1)h],U)\\ \mathbf{u}(kh)=\mathbf{u}_k, \mathbf{u}((k+1)h)=\mathbf{u}_{k+1}}} \sum_{n=1}^{m} w_n L\left(\sum_{\nu=0}^{s} \mathbf{u}_k^\nu \phi_\nu(\tau_n), \sum_{\nu=0}^{s} \mathbf{u}_k^\nu \dot{\phi}_\nu(\tau_n)\right).$$

The discrete Lagrangian maps obtained from this type of discrete Lagrangian are referred as Galerkin variational integrators. It should be noted that the approximation accuracy of the exact discrete Lagrangian is determined by both the order of the interpolation and the order of the quadrature rule. Practically, for a given interpolation function, one should choose a quadrature rule with comparable approximation error. One may refer to [12] for a more in-depth discussion of this issue.

3.3. Spectral variational integrators

Spectral variational integrators (SVI) in this paper are constructed by using the basis functions $\phi_\nu(t) = l_\nu(t)$, where $l_\nu(t)$ are Lagrange interpolation polynomials, and the Gauss–Legendre quadrature rules. Chebyshev and Legendre points will be of particular interest throughout our discussion.

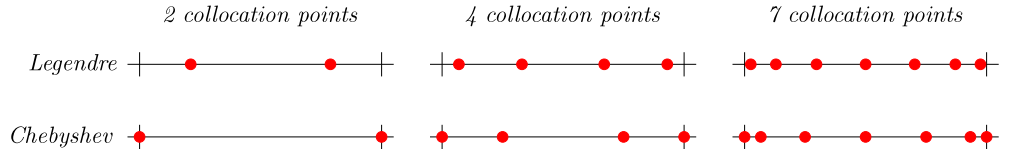

Despite the geometric-structure preserving property, one may also observe that SVI is stable for very large time-steps and converges very fast [12].

3.3.1. Approximation of the exact discrete Lagrangian

To approximate the exact discrete Lagrangian, we should first approximate the variables $\mathbf{u} : [0, T] \to U$. We divide the total time interval $[0, T]$ into M subintervals of equal length h,

$$[0, T] = \bigcup_{k=0}^{M-1} [kh, (k+1)h], \quad M = T/h,$$

and then approximate the exact discrete Lagrangian $L_d^E(\mathbf{u}_k, \mathbf{u}_{k+1})$ with a highly-accurate and numerically computable discrete Lagrangian $L_d(\mathbf{u}_k, \mathbf{u}_{k+1})$. To be specific, for a given Lagrangian functional $L : TU \to \mathbb{R}$, we approximate the infinite-dimensional function space,

$$\mathcal{C}([kh, (k+1)h], U) = \{\mathbf{u} \in C^2([kh, (k+1)h], U) \mid \mathbf{u}(kh) = \mathbf{u}_k, \mathbf{u}((k+1)h) = \mathbf{u}_{k+1}\},$$

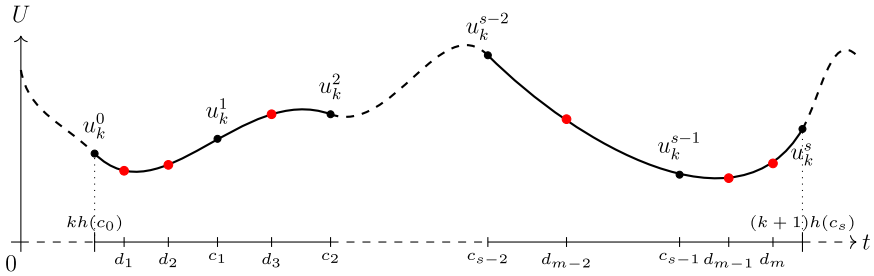

Fig. 3. The red dots represent the quadrature points, which may or may not be the same as the interpolation points which represented by black dots. (For interpretation of the references to color in this figure legend, the reader is referred to the web version of this article.)

with a finite-dimensional function subspace,

$$\mathcal{C}^s([kh,(k+1)h],U)=\{\mathbf{u}\in\mathcal{C}([kh,(k+1)h],U)\mid \mathbf{u}\text{ is a polynomial of degree }s\}.^{1}$$

As illustrated in Fig. 3, we approximate the exact discrete Lagrangian by a s-degree polynomial generated by Lagrangian interpolating polynomials based on the Chebyshev points $c_\nu=\frac{(2k+1)h}{2}+\frac{h}{2}\sin\left(\frac{\pi(s-2\nu)}{2s}\right)$, where c_ν are the Chebyshev points,[2] $x_\nu=\sin\left(\frac{\pi(s-2\nu)}{2s}\right)$, $0\le\nu\le s$, rescaled and shifted from $[-1,1]$ to $[kh,(k+1)h]$. Then, for any chosen Gauss–Legendre quadrature formula $(w_n,\tau_n)_{n=1}^m$ in the interval $[-1,1]$, where w_n are the quadrature weights and $\tau_n\in[-1,1]$ are the quadrature points, we obtain approximations of the function $\mathbf{u}$ at the quadrature points d_n,

$$\mathbf{u}(d_n;\mathbf{u}_k^\nu,h)=\sum_{\nu=0}^{s}\mathbf{u}_k^\nu l_{\nu,s}(\tau(d_n)),$$

$$\dot{\mathbf{u}}(d_n;\mathbf{u}_k^\nu,h)=\sum_{\nu=0}^{s}\mathbf{u}_k^\nu \dot{l}_{\nu,s}(\tau(d_n))\frac{\mathrm{d}\tau}{\mathrm{d}t}=\frac{2}{h}\sum_{\nu=0}^{s}\mathbf{u}_k^\nu \dot{l}_{\nu,s}(\tau(d_n)),$$

where $\tau(t)=\frac{2}{h}(t-t_k)-1\in[-1,1]$, d_n are the quadrature points in the interval $[t_k,t_{k+1}]$, and $l_{\nu,s}(\tau)$ are the Lagrange basis polynomials of degree s, $l_{\nu,s}(\tau):[-1,1]\to\mathbb{R}$, that are given by

$$l_{\nu,s}(\tau)=\prod_{0\le j\le s,j\ne\nu}\frac{\tau-x_j}{x_\nu-x_j}.$$

Then, we can approximate the discrete Lagrangian as follows

$$\begin{aligned}L_d(\mathbf{u}_k=\mathbf{u}_k^0,\mathbf{u}_k^1,\ldots,\mathbf{u}_k^{s-1},\mathbf{u}_k^s=\mathbf{u}_{k+1};h)&=\operatorname*{ext}_{\substack{\mathbf{u}\in\mathcal{C}^s([kh,(k+1)h],U)\\ \mathbf{u}_k^0=\mathbf{u}_k,\mathbf{u}_k^s=\mathbf{u}_{k+1}}}\frac{h}{2}\sum_{n=1}^{m}w_n L\left(\mathbf{u}\left(d_n;\mathbf{u}_k^\nu,h\right),\dot{\mathbf{u}}\left(d_n;\mathbf{u}_k^\nu,h\right)\right)\\&=\operatorname*{ext}_{\substack{(\mathbf{u}_k^0,\mathbf{u}_k^1,\ldots,\mathbf{u}_k^{s-1},\mathbf{u}_k^s)\\ \mathbf{u}_k^0=\mathbf{u}_k,\mathbf{u}_k^s=\mathbf{u}_{k+1}}}\frac{h}{2}\sum_{n=1}^{m}w_n L\left(\sum_{\nu=0}^{s}\mathbf{u}_k^\nu l_{\nu,s}(\tau_n),\frac{2}{h}\sum_{\nu=0}^{s}\mathbf{u}_k^\nu \dot{l}_{\nu,s}(\tau_n)\right).\end{aligned}\tag{14}$$

Remark 3.1. We have chosen Chebyshev interpolation as the Chebyshev points include the boundary points at kh and $(k+1)h$, and the use of Lagrange polynomials that include the boundary points as interpolation points dramatically simplifies the computation of the discrete Legendre transforms $D_1L(q_k,q_{k+1})$ and $D_2L(q_k,q_{k+1})$. Unlike Lagrange interpolants based on equidistant points, it does not exhibit Runge's phenomenon. The choice of Gaussian quadrature is mainly motivated by the optimal accuracy. In particular, an n-point Gaussian quadrature rule is exact for polynomials of degree $2n-1$. However, it would also be worth considering other kinds of polynomial bases and quadrature rules. For example, Galerkin variational integrators based on polynomials of degree n and Gauss–Legendre quadrature rule of order n are shown to result in the Gauss–Legendre collocation methods of order $2n$ [15]. While we have primarily discussed the approximation of the quadrature that only depends on the integrand, one could also consider quadrature formulas that depend on derivatives of the integrand. Different combinations of polynomial bases and quadrature formulas may lead to effective integrators for specific kinds of equations.

[1] Since $\mathbf{u}$ is a vector, we mean that each component of $\mathbf{u}$ is a polynomial of degree s.

[2] We change the conventional Chebyshev points $x_\nu=\cos(\frac{\nu\pi}{s})$ to this form by using the identity $\cos(\theta)=\sin(\frac{\pi}{2}-\theta)$. In floating-point arithmetic, Chebyshev points that are computed using this formula are more symmetric about the origin than the conventional one [18].

3.3.2. Implementation of spectral variational integrators for multi-dimensional Hamiltonian ODEs

From (14), we know that the quadrature approximation of the action integral is stationary with respect to the internal stages $\mathbf{u}_k^\nu$, $\nu = 1, \ldots, s-1$, which provides $(N-1) \times (s-1)$ equations[3]:

$$D_i L_d(\mathbf{u}_k^0, \mathbf{u}_k^1, \ldots, \mathbf{u}_k^{s-1}, \mathbf{u}_k^s; h) = 0, \quad i = 1, \ldots, s-1,$$

which when combined with either the discrete Euler–Lagrange equations,

$$D_s L_d(\mathbf{u}_{k-1} = \mathbf{u}_{k-1}^0, \mathbf{u}_{k-1}^1, \ldots, \mathbf{u}_{k-1}^{s-1}, \mathbf{u}_{k-1}^s = \mathbf{u}_k; h) + D_0 L_d(\mathbf{u}_k = \mathbf{u}_k^0, \mathbf{u}_k^1, \ldots, \mathbf{u}_k^{s-1}, \mathbf{u}_k^s = \mathbf{u}_{k+1}; h) = 0,$$

or the implicit discrete Euler–Lagrange equations (here, $D_i L_d$ means the partial derivative of L_d with respect to $\mathbf{u}_k^i$),

$$\begin{aligned}
\mathbf{p}_k &= -D_0 L_d(\mathbf{u}_k = \mathbf{u}_k^0, \mathbf{u}_k^1, \ldots, \mathbf{u}_k^{s-1}, \mathbf{u}_k^s = \mathbf{u}_{k+1}; h),\\
\mathbf{p}_{k+1} &= D_s L_d(\mathbf{u}_k = \mathbf{u}_k^0, \mathbf{u}_k^1, \ldots, \mathbf{u}_k^{s-1}, \mathbf{u}_k^s = \mathbf{u}_{k+1}; h),
\end{aligned}$$

yields the following set of nonlinear equations:

$$\begin{aligned}
\mathbf{p}_k = -\sum_{n=1}^{m} w_n \Bigg[&\frac{h}{2} l_{0,s}(\tau_n) \frac{\partial L}{\partial \mathbf{u}} \Big(\sum_{\nu=0}^{s} \mathbf{u}_k^\nu l_{\nu,s}(\tau_n), \frac{2}{h} \sum_{\nu=0}^{s} \mathbf{u}_k^\nu \dot{l}_{\nu,s}(\tau_n) \Big)\\
&+ \dot{l}_{0,s}(\tau_n) \frac{\partial L}{\partial \dot{\mathbf{u}}} \Big(\sum_{\nu=0}^{s} \mathbf{u}_k^\nu l_{\nu,s}(\tau_n), \frac{2}{h} \sum_{\nu=0}^{s} \mathbf{u}_k^\nu \dot{l}_{\nu,s}(\tau_n) \Big) \Bigg], \qquad (15)\\
\mathbf{0} = \sum_{n=1}^{m} w_n \Bigg[&\frac{h}{2} l_{r,s}(\tau_n) \frac{\partial L}{\partial \mathbf{u}} \Big(\sum_{\nu=0}^{s} \mathbf{u}_k^\nu l_{\nu,s}(\tau_n), \frac{2}{h} \sum_{\nu=0}^{s} \mathbf{u}_k^\nu \dot{l}_{\nu,s}(\tau_n) \Big)\\
&+ \dot{l}_{r,s}(\tau_n) \frac{\partial L}{\partial \dot{\mathbf{u}}} \Big(\sum_{\nu=0}^{s} \mathbf{u}_k^\nu l_{\nu,s}(\tau_n), \frac{2}{h} \sum_{\nu=0}^{s} \mathbf{u}_k^\nu \dot{l}_{\nu,s}(\tau_n) \Big) \Bigg], \qquad (16)\\
\mathbf{p}_{k+1} = \sum_{n=1}^{m} w_n \Bigg[&\frac{h}{2} l_{s,s}(\tau_n) \frac{\partial L}{\partial \mathbf{u}} \Big(\sum_{\nu=0}^{s} \mathbf{u}_k^\nu l_{\nu,s}(\tau_n), \frac{2}{h} \sum_{\nu=0}^{s} \mathbf{u}_k^\nu \dot{l}_{\nu,s}(\tau_n) \Big)\\
&+ \dot{l}_{s,s}(\tau_n) \frac{\partial L}{\partial \dot{\mathbf{u}}} \Big(\sum_{\nu=0}^{s} \mathbf{u}_k^\nu l_{\nu,s}(\tau_n), \frac{2}{h} \sum_{\nu=0}^{s} \mathbf{u}_k^\nu \dot{l}_{\nu,s}(\tau_n) \Big) \Bigg], \qquad (17)
\end{aligned}$$

where $r = 1, \ldots, s-1$. The multi-interval algorithm for solving (15), (16), (17) can be obtained by cycling through the following diagram,

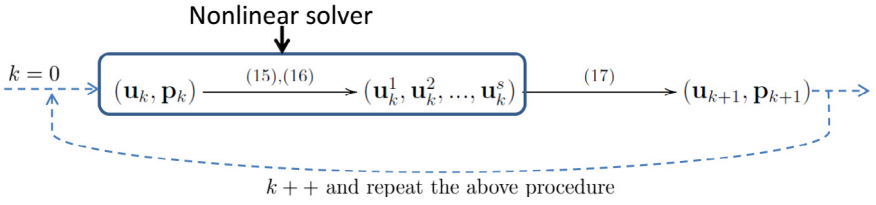

To implement the algorithm efficiently for the semi-discrete equation (9), we give the matrix form of (15), (16) for (9),

$$\tilde{A}_k \tilde{U}_k = F_k, \qquad (18)$$

where $\tilde{A}_k$ is a $s \times (s+1)$ matrix and the entries are given by

$$\tilde{A}_k^{i,j} = \frac{2}{h} \sum_{n=1}^{m} w_n \dot{l}_{i-1,s}(\tau_n) \dot{l}_{j-1,s}(\tau_n), \qquad (19)$$

$\tilde{U}_k$ is a $(s+1) \times (N-1)$-dimensional matrix,

$$\tilde{U}_k = [\mathbf{u}_k^0, \mathbf{u}_k^1, \ldots, \mathbf{u}_k^s]^T, \quad \mathbf{u}_k^\nu = [u_k^\nu(x_1, t), \ldots, u_k^\nu(x_{N-1}, t)].$$

[3] Here, N denotes the dimension of the Hamiltonian system, specifically, we semi-discretize (2) with $N+1$ points, the resultant system of semi-discrete ODEs is of dimension $N-1$, since the boundary conditions are given.

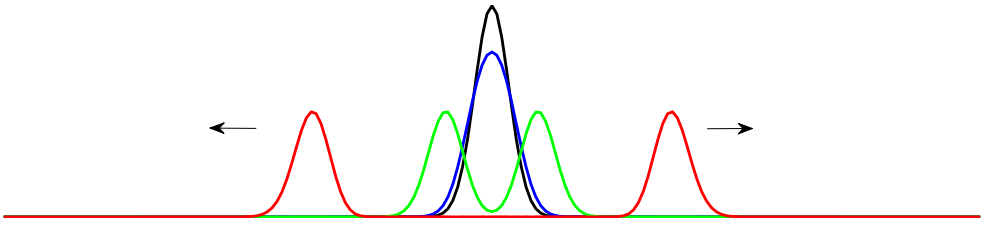

Fig. 4. Evolution of Gaussian wave.

F_k is a $s \times (N-1)$-dimensional matrix,

$$F_k = [\mathbf{f}_k^0, \mathbf{f}_k^1, \ldots, \mathbf{f}_k^{s-1}]^T = \left[\frac{h}{2}\sum_{n=1}^{m} w_n l_{0,s}(\tau_n)\cdot\frac{\partial L}{\partial \mathbf{u}}, \frac{h}{2}\sum_{n=1}^{m} w_n l_{1,s}(\tau_n)\cdot\frac{\partial L}{\partial \mathbf{u}}, \ldots, \frac{h}{2}\sum_{n=1}^{m} w_n l_{s-1,s}(\tau_n)\cdot\frac{\partial L}{\partial \mathbf{u}}\right]^T,$$

where $\frac{\partial L}{\partial \mathbf{u}} = [\frac{\partial L}{\partial u_N(x_1,t)}, \ldots, \frac{\partial L}{\partial u_N(x_{N-1},t)}]$. By using the partitions $\tilde{A}_k = [A_k^1, A_k]$ and $\tilde{U}_k = [\mathbf{u}_k^0, U_k]^T$ where A_k^1 is the first column of the matrix $\tilde{A}_k$, we can rewrite (18) as

$$A_k \otimes I_{N-1}\mathrm{vec}(U_k) + A_k^1 \otimes (\mathbf{u}_k^0)^T + \mathrm{vec}(F_k) = [-\mathbf{p}_k, \mathbf{0}_{(N-1)(s-1)}]^T, \tag{20}$$

where I_{N-1} is the $(N-1)\times(N-1)$ identity matrix. Thus, we can calculate $\mathrm{vec}(U_k)$ from (20) using Newton–Raphson iteration.

4. Error estimation

The error of our numerical approach mainly comes from two parts. One is the approximation of derivative of u with respect to x. The other comes from the chosen spectral variational integrator. Now we recall the geometric convergence of spectral variational integrators. The definition of geometric convergence can be found in papers and monographs about approximation theory [23,24]. Specifically, a sequence of approximations $\{f_n\}_{n=1}^{\infty}$ is said to converge to f geometrically, if,

$$\|f - f_n\| = \mathcal{O}(K^n),$$

for a given norm $\|\cdot\|$ and a positive constant $K < 1$ which is independent of n.

Theorem 4.1 (*Theorem 3.7 of [12]*)**.** *For a canonical Lagrangian and a sufficiently small time-step h, a Galerkin variational integrator constructed from a basis $\{\phi_v\}_{v=0}^{s}$ or polynomials of degree at most s and a quadrature rule of at least order $2s+1$ will have error at most $\mathcal{O}(K^s)$ for some K independent of s and less than 1. The internal stage Euler–Lagrange equations needed to construct the Galerkin variational integrator will also have a unique solution.*

One might argue that spatial semi-discretization using symmetric finite-difference methods renders the use of spectrally accurate in time methods pointless, as one only achieves finite-order spatial accuracy, whereas the SVI is spectral accurate in time. But, we will see in practice that the numerical method can reach near machine precision with the given high-order symmetric difference and a relative small spatial-step.

Theorem 4.2. *Suppose $u(x,t)$ is the exact solution of the Hamiltonian wave equation (2) and denote by $\hat{\mathbf{u}} = (\hat{u}_0, \hat{u}_1, \ldots, \hat{u}_N)^T$ the solution of the semi-discrete equation (3) with the pth order symmetric difference matrix D solved by spectral variational integrators with a fixed time-step h and s-dimensional approximation space. Then, for any space grid x_i, $i = 0, \ldots, N$ and $t \in [0, h]$, we have,*

$$|u(x_i,t) - \hat{u}_i(t)| \le C_0(\Delta x)^p + C_1 K^s, \quad i = 0, \ldots, N$$

for some positive constants C_0, C_1, $0 < K < 1$, $\Delta x < 1$.

Proof. By introducing the notation $\mathbf{u}(t) = (u_0(t), u_1(t), \ldots, u_N(t))^T$ which denotes the exact solution of the semi-discrete equation (3), Theorem 4.2 can be easily obtained from Theorem 4.1 by using the triangle inequality. □

5. Numerical examples

In this section, we will introduce two numerical examples to verify the numerical schemes described above. The first example is the one-dimensional linear wave equation with an initial Gaussian pulse. The Gaussian pulse will eventually decay into two waves with smaller amplitude, with equal but opposite velocities (see Fig. 4).

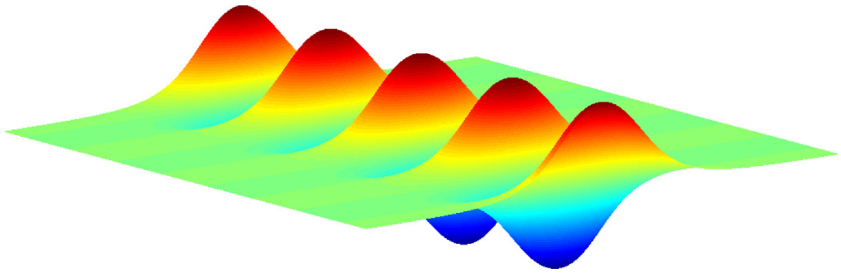

Fig. 5. Breather solution of sine-Gordon equation.

For the second example, we consider the solitonic breather solution of the sine-Gordon equation. The sine-Gordon equation describes nonlinear waves in elastic media which can be solved analytically for some initial conditions, since it is completely integrable. The form of the breather solution is shown in Fig. 5.

For each example, the spectral variational integrators were constructed by using Chebyshev-Lagrangian interpolation and Gauss–Legendre quadrature.

5.1. The Gaussian wave

We consider the linear wave equation,

$$\frac{\partial^2 u}{\partial t^2} - \frac{\partial^2 u}{\partial x^2} = 0,$$

with an initial Gaussian pulse,

$$\begin{cases} u(x, 0) = \exp(-x^2), \\ u_t(x, 0) = 0. \end{cases}$$

The analytic solution of the linear wave equation is,

$$u(x, t) = \frac{1}{2}\left\{\exp\left[-(x+t)^2\right] + \exp\left[-(x-t)^2\right]\right\}.$$

Figs. 6 and 7 show the numerical solution, error and energy error of the second-order semi-discrete wave equation solved by SVI with 5 point Chebyshev interpolation, 10 point Gauss–Legendre quadrature and fixed time-step $\Delta t = 1$. The energy we calculated here was given in (7) and the energy error is the plot of $H(\mathbf{u}, \dot{\mathbf{u}}) - H(\mathbf{u}_0, \dot{\mathbf{u}}_0)$. Figs. 8 and 9 give the numerical solution, error and energy error of the 4th-order symmetric-difference semi-discrete wave equation solved by SVI with 7 point Chebyshev interpolation and 14 point Gauss–Legendre quadrature at every time-step, and Figs. 10 and 11 are for the 8th-order symmetric difference with 11 point Chebyshev interpolation and 22 point Gauss–Legendre quadrature at every time-step. Here, we show the solution and absolute error at the first time-step. The long-time behavior of the solution will be given in the following comparison between numerical schemes derived from SVI and multisymplectic variational integrators. The long-time energy errors are obtained by solving the linear wave equation with the homogeneous boundary condition $u(-5, t) = u(5, t) = 0$. Comparisons of the numerical schemes proposed in this paper and the multisymplectic variational integrator (MVI) (5.8) in [4]

$$\frac{u_{i+1,j} - 2u_{i,j} + u_{i-1,j}}{k^2} - \frac{u_{i,j+1} - 2u_{i,j} + u_{i,j-1}}{h^2} + \frac{1}{3}V'\left(\frac{u_{i,j} + u_{i,j+1} + u_{i+1,j+1}}{3}\right) + \frac{1}{3}V'\left(\frac{u_{i,j-1} + u_{i,j} + u_{i+1,j}}{3}\right) + \frac{1}{3}V'\left(\frac{u_{i-1,j-1} + u_{i-1,j} + u_{i,j}}{3}\right) = 0 \tag{21}$$

for relative long-time simulations are shown in Table 2. For the linear wave equation, the above MVI scheme reduces to the leap-frog scheme which has truncation error $\mathcal{O}(\Delta x^2 + \Delta t^2)$. The comparison of SVI and MVI is motivated by the fact that both schemes are deeply rooted in Lagrangian mechanics and they both exhibit good energy behavior. Some approaches for constructing higher-order multisymplectic variational integrators have been summarized in [13], such as multisymplectic variational integrator constructed by using tensor product linear shape functions with localized supports to discretize the configuration bundle, spatio-temporally adaptive variational integrators and pseudospectral variational integrators. However, the constructions and implementations of these methods are relatively complicated. As such, we only compare our method with (21) and we choose a relative large spatial domain $x \in [-15, 15]$ to avoid the error induced by the boundary and the discretization of the boundary condition.

The numerical results demonstrate that MVI is not as efficient for high-accuracy simulations, because of both the computational and storage complexity. In particular, although the MVI is explicit for the linear wave equation ($V' = 0$), we still observe that SVI_SD6 and SVI_SD8 achieve higher accuracy at a lower computational cost when compared to MVI.

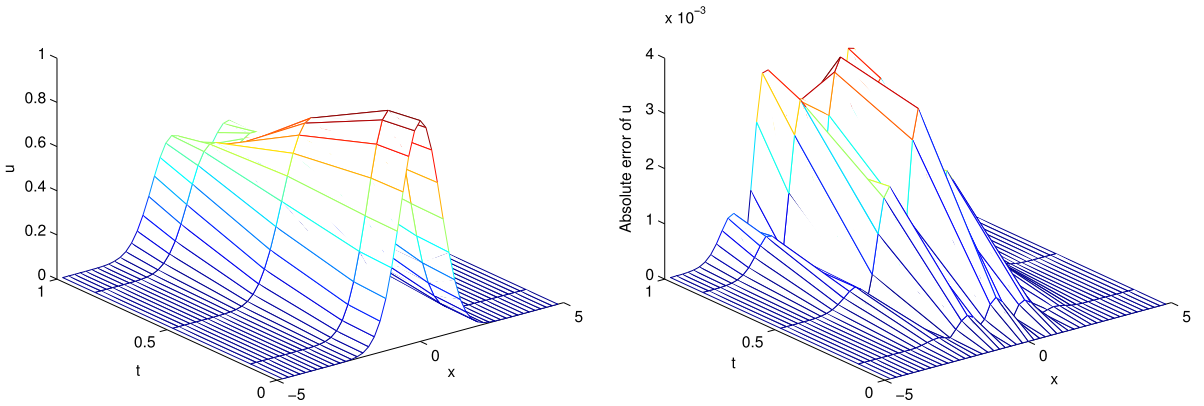

Fig. 6. Solution (left) and error (right) for the linear wave equation using SVI for the second-order semi-discrete ODEs on a space–time grid with $\Delta t = 1$, $\Delta x = 0.2$ and 5 point Chebyshev interpolation, 10 point Gauss–Legendre quadrature at every time-step.

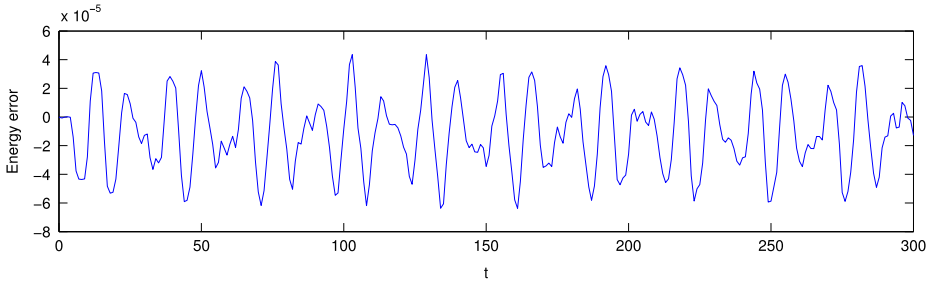

Fig. 7. Energy error for the linear wave equation using SVI for the second-order semi-discrete ODEs on a space–time grid with $\Delta t = 1$, $\Delta x = 0.2$ and 5 point Chebyshev interpolation and 10 point Gauss–Legendre quadrature at every time-step.

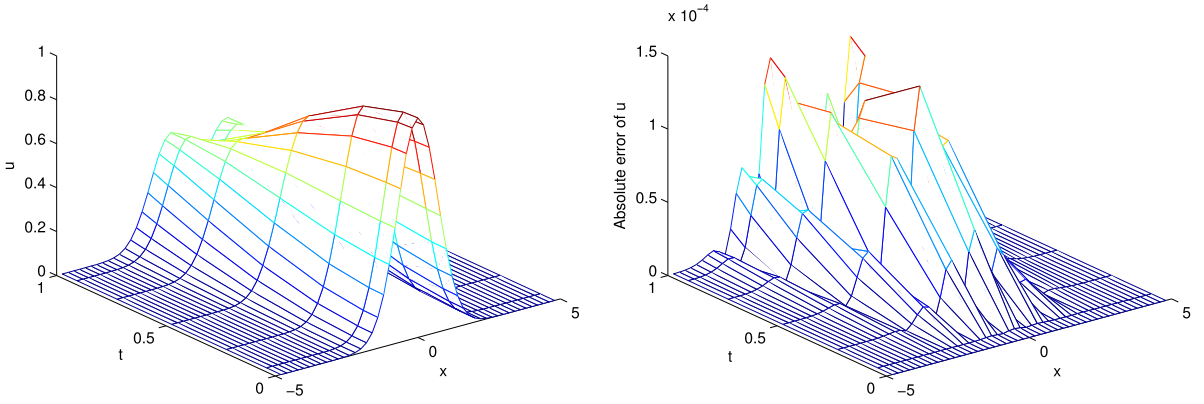

Fig. 8. Solution (left) and error (right) for the linear wave equation using SVI for the 4th-order semi-discrete ODEs on a space–time grid with $\Delta t = 1$, $\Delta x = 0.2$ and 7 point Chebyshev interpolation, 14 point Gauss–Legendre quadrature at every time-step.

Table 2
Computational Efficiency of MVI, SVI_SD6 and SVI_SD8.

Method	Scheme detail				Total time (s)	Error[a]	CPU-time (s)
	Δx	Δt	Chebyshev	Legendre			
MVI[b]	0.001	0.0005	–	–	10	6.099×10^{-7}	146.83
SVI_SD6[c]	0.06	1	7	12	10	3.335×10^{-7}	98.23
SVI_SD8	0.1	1	7	12	10	2.939×10^{-7}	31.56

[a] Maximum absolute error in the space–time grid.
[b] For the linear wave equation, MVI reduces to the leap-frog method.
[c] Spectral variational integrator for the 6th-order spatial semi-discrete ODEs.

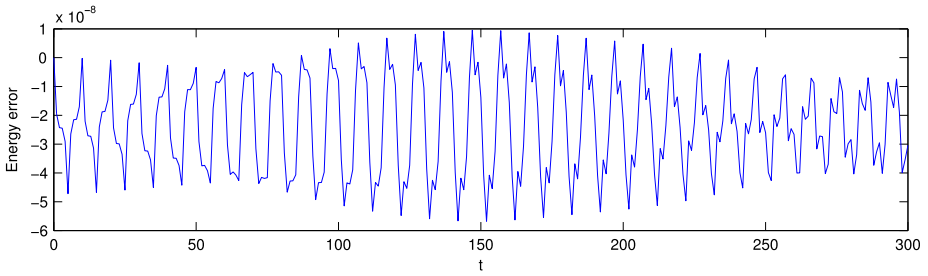

Fig. 9. Energy error for the linear wave equation using SVI for the 4th-order semi-discrete ODEs on a space–time grid with $\Delta t = 1$, $\Delta x = 0.2$ and 7 point Chebyshev interpolation, 14 point Gauss–Legendre quadrature at every time-step.

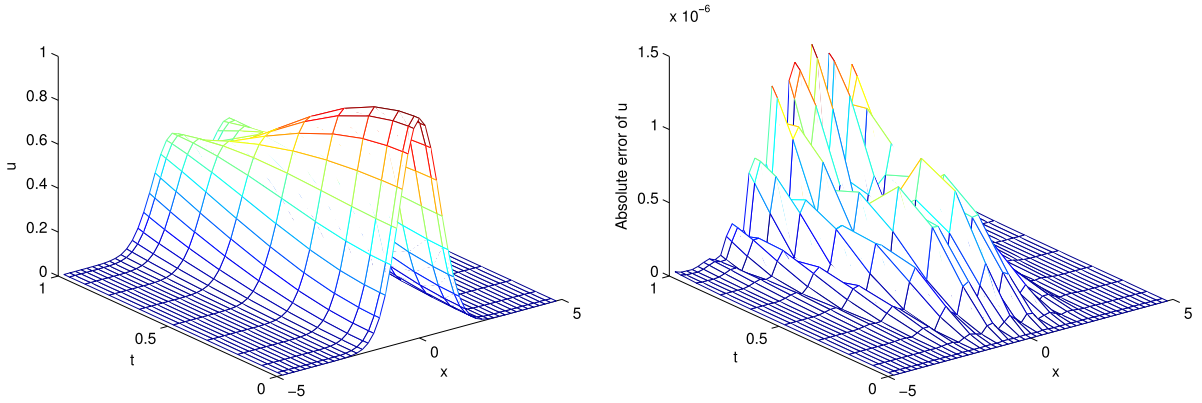

Fig. 10. Solution (left) and error (right) for the linear wave equation using SVI for the 8th-order semi-discrete ODEs on a space–time grid with $\Delta t = 1$, $\Delta x = 0.2$ and 11 point Chebyshev interpolation, 22 point Gauss–Legendre quadrature at every time-step.

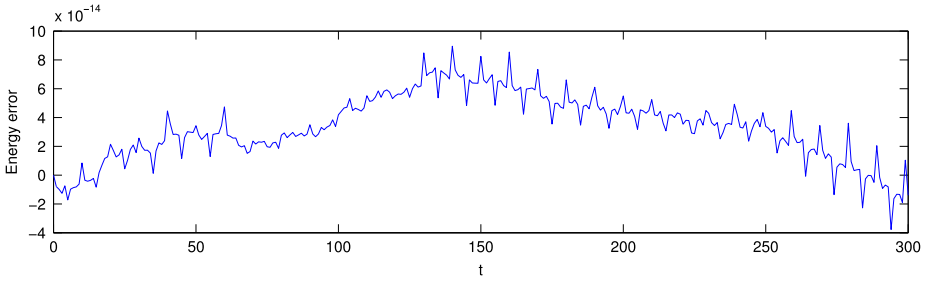

Fig. 11. Energy error for the linear wave equation using SVI for the 8th-order semi-discrete ODEs on a space–time grid with $\Delta t = 1$, $\Delta x = 0.2$ and 11 point Chebyshev interpolation, 22 point Gauss–Legendre quadrature at every time-step.

We can also see that methods proposed in this paper are stable for large time-steps, while MVI is actually a finite-difference method which need to satisfy the Courant–Friedrichs–Lewy (CFL) condition when solving hyperbolic partial differential equations. Figs. 12 and 13 give the solution and absolute error of the linear wave equation solved by SVI_SD6 and SVI_SD8. We do not include the simulation figure of MVI, as the figure is too large due to the very small Δx and Δt that are necessary in order to achieve comparable accuracy.

Fig. 14 shows the L^∞ error of u (left) and energy error (right) of the 8th-order semi-discrete equation with three different spatial-steps $\Delta x = 0.5$, $\Delta x = 0.2$, $\Delta x = 0.1$, solved by SVI with different numbers of Chebyshev points. The number of quadrature points is chosen to be two times the number of Chebyshev points. It is clear that for an extreme accurate SVI, the order of the spatial semi-discretization is the limiting factor in the overall numerical accuracy, just as we discussed in the last section. But we can still achieve very high accuracy with higher-order semi-discretizations. The discrete energy error mainly depends on the number of Chebyshev points we choose, since it is an exact integral of motion of the semi-discrete equations.

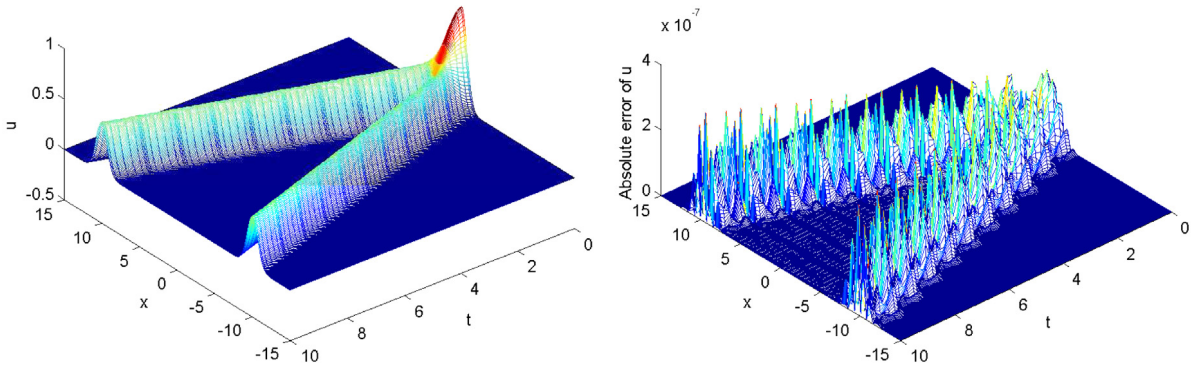

Fig. 12. Solution (left) and error (right) for the linear wave equation using SVI_SD6.

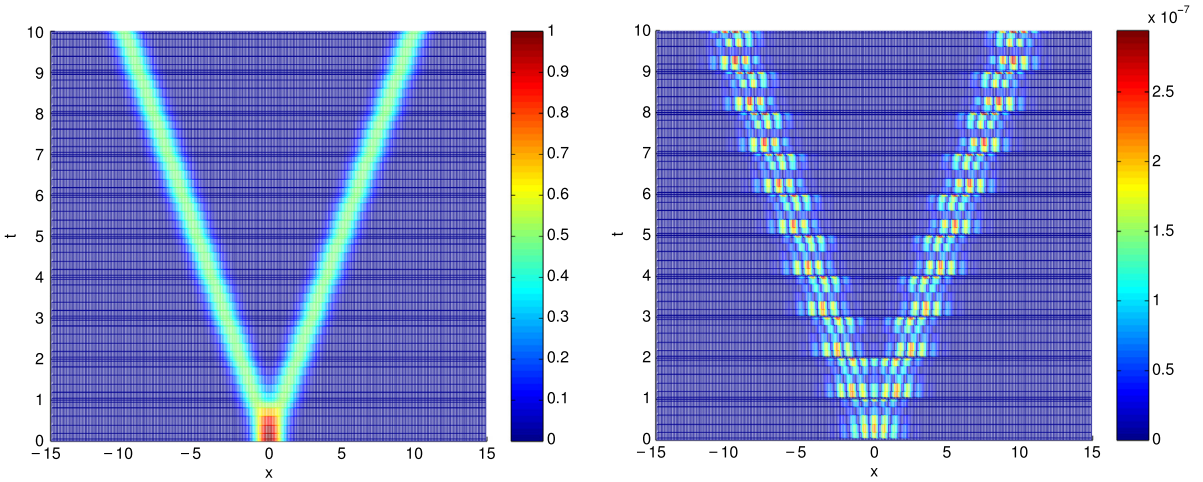

Fig. 13. Solution (left) and error (right) for the linear wave equation using SVI_SD8.

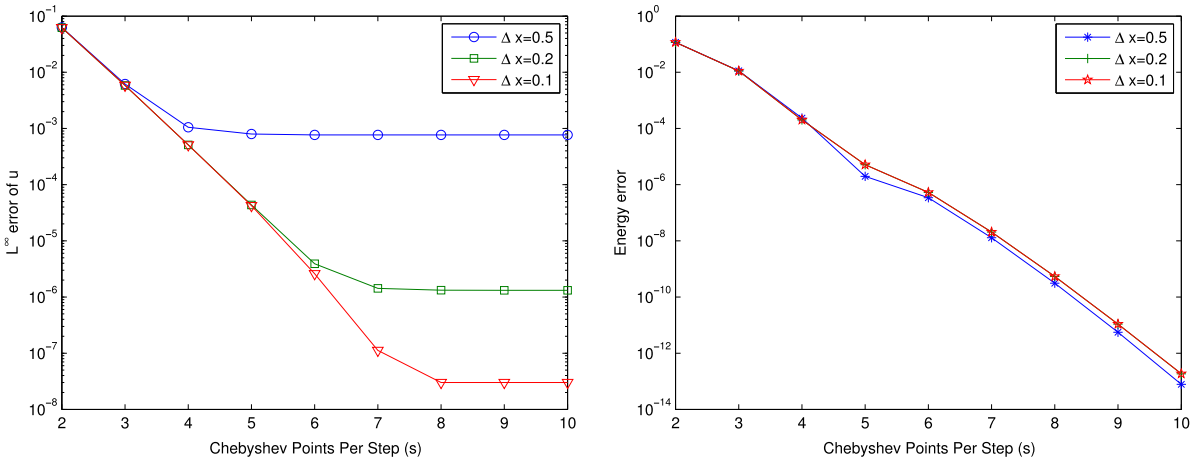

Fig. 14. L^{∞} error of u (left) and absolute energy error (right) at $t = 1$ of the linear wave equation when using SVI for the 8th-order semi-discrete ODEs with s-refinement (s is the number of Chebyshev points), here $\Delta t = 1$.

5.2. The sine-Gordon equation

Now we consider the sine-Gordon equation, which is in the form,

$$\frac{\partial^2 u}{\partial t^2} = \frac{\partial^2 u}{\partial x^2} - \sin(u(x,t)), \quad x \in [-30, 30], \ t \geq 0. \tag{22}$$

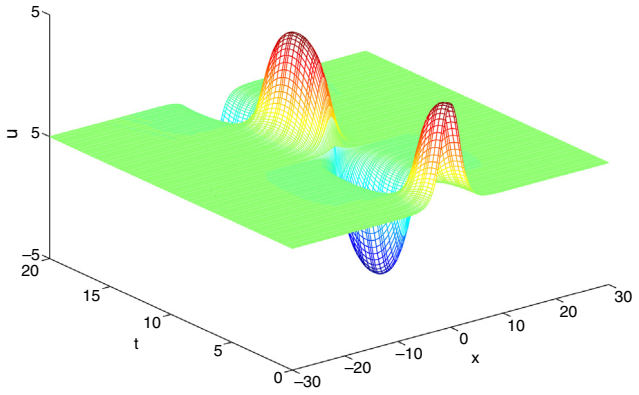

Fig. 15. Solution of the sine-Gordon equation using SVI for the 4th-order semi-discrete ODEs on a space–time grid with $\Delta t = 1$, $\Delta x = 0.2$ and 5 point Chebyshev interpolation, 10 point Gauss–Legendre quadrature at every time-step.

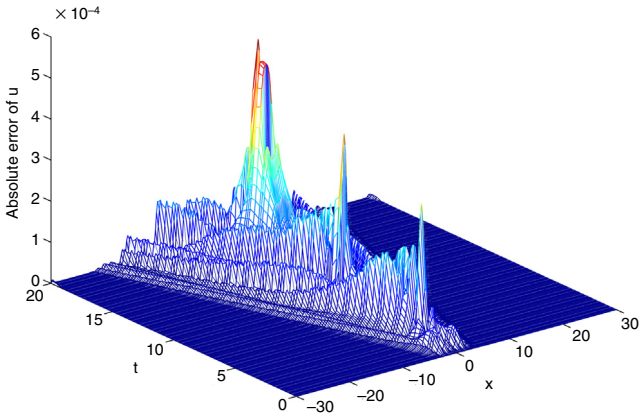

Fig. 16. Absolute error of u for the sine-Gordon equation using SVI for the 4th-order semi-discrete ODEs on a space–time grid with $\Delta t = 1$, $\Delta x = 0.2$ and 5 point Chebyshev interpolation, 10 point Gauss–Legendre quadrature at every time-step.

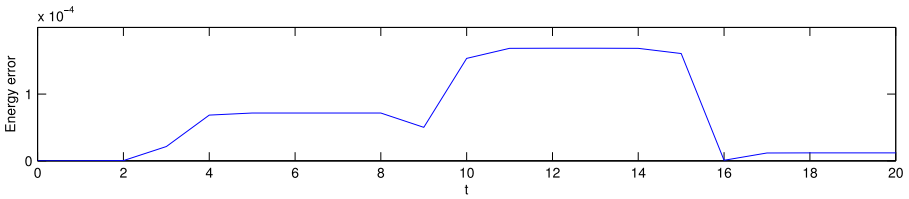

Fig. 17. Energy error for the sine-Gordon equation using SVI for the 4th-order semi-discrete ODEs on a space–time grid with $\Delta t = 1$, $\Delta x = 0.2$ and 5 point Chebyshev interpolation, 10 point Gauss–Legendre quadrature at every time-step.

Here, we consider the so-called breather solutions with the initial conditions,

$$u(x, 0) = 4\tan^{-1}\left(\frac{\sqrt{1-w^2}}{w}\frac{1}{\cosh(x\sqrt{1-w^2})}\right), \quad u_t = 0,$$

and Dirichlet boundary conditions which can be obtained from the given exact solution,

$$u(x, t) = 4\tan^{-1}\left(\frac{\sqrt{1-w^2}}{w}\frac{\cos(wt)}{\cosh(x\sqrt{1-w^2})}\right).$$

Figs. 15–17, respectively give the solution, absolute error and energy error of the 4th-order semi-discrete sine-Gordon equation when solved by SVI with 5 point Chebyshev interpolation and 10 point Gauss–Legendre quadrature at every time-step with uniform $\Delta t = 1$.

Fig. 18 shows the L^∞ error of u for the 8th-order semi-discrete sine-Gordon equation with four different spatial-steps $\Delta x = 0.5$, $\Delta x = 0.2$, $\Delta x = 0.05$, $\Delta x = 0.02$, solved by SVI as the number of Chebyshev points is allowed to vary. The

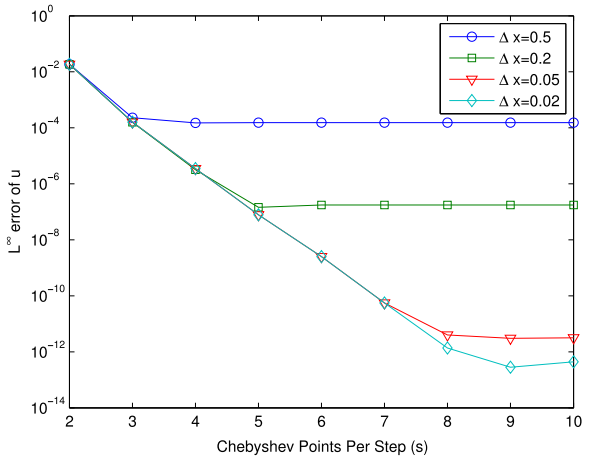

Fig. 18. L^∞ error of u at $t = 1$ of the sine-Gordon equation when using SVI for the 8th-order semi-discrete ODEs with s-refinement (s is the number of Chebyshev points), here $\Delta t = 1$.

number of quadrature points is chosen to be two times the number of Chebyshev points. Combined with the high-order semi-discretization and a relative small spatial-step, SVI can achieve very high accuracy for the Hamiltonian PDEs, while the implicit scheme of MVI is extremely inefficient with small size space–time grid, especially for equations with large spatial domain.

Exponential time differencing (ETD) methods can not only solve the linear part of the semi-discrete equations exactly, but also preserve the underlying group structure. Now, we compare SVI with a class of exponential time differencing Runge–Kutta methods (ETDRK) which were derived in the paper by Cox and Matthews [25] for ordinary differential equations with stiff linear parts. These kinds of methods have relative small error constants and are exact for linear part of the differential equation. It was also pointed out in the paper by Kassam and Trefethen [26] that ETDRK consistently outperforms the implicit–explicit method (IMEX), the split step method (SS), the integrating factor method (IF) and the slider method (SL) in accuracy, efficiency and stability when tested on the KdV, Kuramoto–Sivashinsky, Burgers and Allen–Cahn equations in one space dimension. For the sine-Gordon equation, we first discretize the spatial part of the PDE and obtain a system of ODEs,

$$u_{tt} = \mathbf{L}u + \mathbf{N}(u, t), \tag{23}$$

then, we convert the second-order system (23) into a first-order system by introducing the auxiliary variable $v = u'$,

$$\begin{cases} u_t = v, \\ v_t = \mathbf{L}u + \mathbf{N}(u, t). \end{cases} \tag{24}$$

Let $Z = [u, v]^T$, then Eq. (24) can be expressed in the following standard form which can be solved by ETDRK methods directly,

$$Z_t = \mathbf{A}Z + \mathbf{N}(Z, t), \tag{25}$$

where

$$\mathbf{A} = \begin{pmatrix} \mathbf{0} & \mathbf{I} \\ \mathbf{L} & \mathbf{0} \end{pmatrix}, \qquad \mathbf{N}(Z, t) = \begin{pmatrix} \mathbf{0} \\ \mathbf{N}(u, t) \end{pmatrix}.$$

The fourth-order scheme ETD4RK for (25) is,

$$\begin{aligned}
\alpha_n &= e^{\mathbf{A}h/2} Z_n + \mathbf{A}^{-1}(e^{\mathbf{A}h/2} - \mathbf{I})\mathbf{N}(Z_n, t_n), \\
\beta_n &= e^{\mathbf{A}h/2} Z_n + \mathbf{A}^{-1}(e^{\mathbf{A}h/2} - \mathbf{I})\mathbf{N}(\alpha_n, t_n + h/2), \\
\gamma_n &= e^{\mathbf{A}h/2} \alpha_n + \mathbf{A}^{-1}(e^{\mathbf{A}h/2} - \mathbf{I})(2\mathbf{N}(\beta_n, t_n + h/2) - \mathbf{N}(Z_n, t_n)), \\
Z_{n+1} &= e^{\mathbf{A}h} Z_n + h^{-2}\mathbf{A}^{-3}\{[-4 - \mathbf{A}h + e^{\mathbf{A}h}(4 - 3\mathbf{A}h + (\mathbf{A}h)^2)]\mathbf{N}(Z_n, t_n) \\
&\quad + 2[2 + \mathbf{A}h + e^{\mathbf{A}h}(-2 + \mathbf{A}h)](\mathbf{N}(\alpha_n, t_n + h/2) + \mathbf{N}(\beta_n, t_n + h/2)) \\
&\quad + [-4 - 3\mathbf{A}h - (\mathbf{A}h)^2 + e^{\mathbf{A}h}(4 - \mathbf{A}h)]\mathbf{N}(\gamma_n, t_n + h)\}.
\end{aligned}$$

To implement the ETD4RK methods, we should first resolve the spatial part of the problem to very high accuracy with spectral methods or finite differences. To compare the ETDRK methods with SVI, we use symmetric differences to discretize the spatial part of (22), which makes $\mathbf{A}$ a sparse, nondiagonal and large-scale matrix. For example, the dimension of $\mathbf{A}$ is

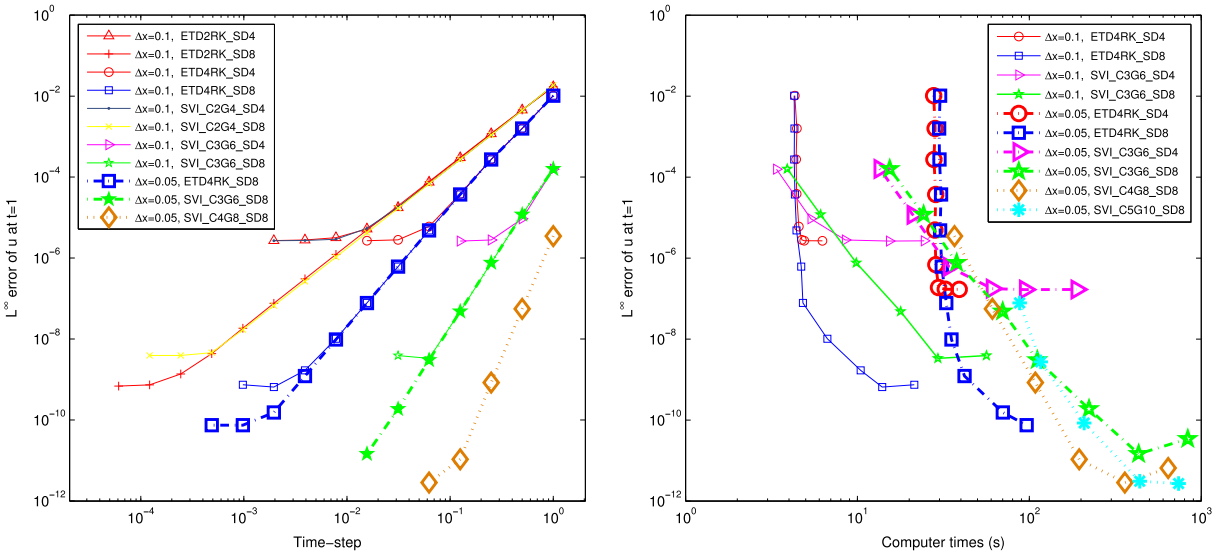

Fig. 19. Accuracy versus time step and computer time for the sine-Gordon equation. (Here ETD2RK_SD4 denotes the ETD2RK method for the fourth-order semi-discrete ODEs and SVI_C2G4_SD4 denotes SVI with 2 point Chebyshev interpolation and 4 point Gauss–Legendre quadrature for the fourth-order semi-discrete ODEs.)

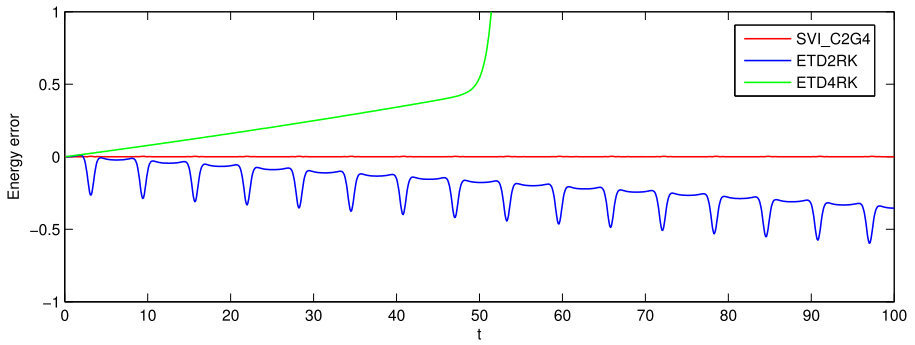

Fig. 20. Comparison of the energy behaviors of ETDRK and SVI for the fourth-order semi-discrete sine-Gordon equation with $\Delta t = 0.1$ and $\Delta x = 0.1$.

2400×2400, when we set the spatial step $\Delta x = 0.05$ in the spatial domain $[-30, 30]$. Several approaches have been introduced to deal with the computation of $e^{\mathbf{A}}$, such as Taylor series [25], contour integral [26], Padé approximation [27], scaling and squaring [28], and Krylov subspace approximation [29,30]. The Taylor series is applicable when $\mathbf{A}$ is scalar or a diagonal matrix. The contour integration does not work well with equation (25), probably because we should choose a large contour when the eigenvalue of $\mathbf{A}$ is large and ETD4RK methods implemented in this way are relatively slow due to the need to compute a large number of matrix inverses in order to approximate the complex integration. ETD4RK schemes used in this paper are implemented by using the Padé approximation of matrix exponential functions [27].

As seen in Figs. 19 and 20, we observe that the resulting explicit ETDRK schemes are effective and efficient, but they are not energy preserving. In contrast, SVI methods proposed in this paper preserve the energy of the system very well and can achieve arbitrary high-order for solving (25) by increasing the number of interpolation points and quadrature points. As a class of implicit energy preserving numerical schemes, they may have better long-time performances than that of ETDRK methods and they are more efficient than some conventional symplectical Gauss–Legendre methods (see Table 1 of [16]). SVI might also be a better choice than ETDRK for dealing with extremely large-scale systems, as the time efficiency of ETDRK decays rapidly as the dimension of the linear part increases. It would be interesting for researchers to develop structure-preserving methods based on the ETD framework.

6. Conclusion

We have demonstrated that the combination of spectral variational integrators with high-order symmetric finite-differences can be successfully applied to simulating Hamiltonian PDEs with very high accuracy. With the given efficient implementation of spectral variational integrators for large-dimensional ODEs, we obtain a fully-discrete scheme for the Hamiltonian wave equations that is highly accurate and nearly energy preserving, and also verify the stability of

SVI for the stiff system of Hamiltonian ODEs arising from semi-discretization. In the future, we will construct overall (space–time) spectrally accurate structure-preserving numerical methods and extend these methods to solve more complicated equations, such as Maxwell's equations with gauge symmetry and higher-dimensional Schrödinger equations.

Acknowledgments

YQL and BYW were supported in part by the National Natural Science Foundation of China Grant No. 11271100 and the Fundamental Research Funds for the Central Universities (Grant No. HIT. IBRSEM. A. 201412). ML was supported in part by NSF Grants CMMI-1029445, DMS-1065972, CMMI-1334759, DMS-1345013, DMS-1411792, and NSF CAREER Award DMS-1010687. The authors would like to thank the referees for the helpful and constructive recommendations.

References

[1] U.M. Ascher, R.I. McLachlan, On symplectic and multisymplectic schemes for the KdV equation, J. Sci. Comput. 25 (1–2) (2005) 83–104. http://dx.doi.org/10.1007/s10915-004-4634-6.
[2] W. Hu, Z. Deng, S. Han, W. Zhang, Generalized multi-symplectic integrators for a class of Hamiltonian nonlinear wave PDEs, J. Comput. Phys. 235 (2013) 394–406. http://dx.doi.org/10.1016/j.jcp.2012.10.032.
[3] Y. Sun, P.S.P. Tse, Symplectic and multisymplectic numerical methods for Maxwell's equations, J. Comput. Phys. 230 (5) (2011) 2076–2094. http://dx.doi.org/10.1016/j.jcp.2010.12.006.
[4] J.E. Marsden, G.W. Patrick, S. Shkoller, Multisymplectic geometry, variational integrators, and nonlinear PDEs, Comm. Math. Phys. 199 (2) (1998) 351–395. http://dx.doi.org/10.1007/s002200050505.
[5] T.J. Bridges, Multi-symplectic structures and wave propagation, Math. Proc. Cambridge Philos. Soc. 121 (1) (1997) 147–190. http://dx.doi.org/10.1017/S0305004196001429.
[6] L. Brugnano, G. Frasca Caccia, F. Iavernaro, Energy conservation issues in the numerical solution of the semilinear wave equation, Appl. Math. Comput. 270 (2015) 842–870. http://dx.doi.org/10.1016/j.amc.2015.08.078.
[7] M.J. Gotay, A multisymplectic framework for classical field theory and the calculus of variations. I. Covariant Hamiltonian formalism, in: Mechanics, Analysis and Geometry: 200 Years after Lagrange, in: North-Holland Delta Ser., North-Holland, Amsterdam, 1991, pp. 203–235.
[8] A. Lew, J.E. Marsden, M. Ortiz, M. West, Asynchronous variational integrators, Arch. Ration. Mech. Anal. 167 (2) (2003) 85–146. http://dx.doi.org/10.1007/s00205-002-0212-y.
[9] T.J. Bridges, S. Reich, Multi-symplectic integrators: numerical schemes for Hamiltonian PDEs that conserve symplecticity, Phys. Lett. A 284 (4–5) (2001) 184–193. http://dx.doi.org/10.1016/S0375-9601(01)00294-8.
[10] J.-B. Chen, M.-Z. Qin, Multi-symplectic Fourier pseudospectral method for the nonlinear Schrödinger equation, Electron. Trans. Numer. Anal. 12 (2001) 193–204. electronic.
[11] R.I. McLachlan, B.N. Ryland, Y. Sun, High order multisymplectic Runge–Kutta methods, SIAM J. Sci. Comput. 36 (5) (2014) A2199–A2226. http://dx.doi.org/10.1137/140958050.
[12] J. Hall, M. Leok, Spectral variational integrators, Numer. Math. 130 (4) (2015) 681–740. http://dx.doi.org/10.1007/s00211-014-0679-0.
[13] M. Leok, Generalized Galerkin variational integrators:Lie group, multiscale, and pseudospectral methods, 2004. Preprint arXiv:math.NA/0508360.
[14] M. Leok, T. Shingel, General techniques for constructing variational integrators, Front. Math. China 7 (2) (2012) 273–303. http://dx.doi.org/10.1007/s11464-012-0190-9.
[15] J.E. Marsden, M. West, Discrete mechanics and variational integrators, Acta Numer. 10 (2001) 357–514. http://dx.doi.org/10.1017/S096249290100006X.
[16] Yiqun Li, Boying Wu, Melvin Leok, Spectral-collocation variational integrators, J. Comput. Phys. 332 (2017) 83–98. http://dx.doi.org/10.1016/j.jcp.2016.12.007.
[17] P. Amodio, I. Sgura, High-order finite difference schemes for the solution of second-order BVPs, J. Comput. Appl. Math. 176 (1) (2005) 59–76. http://dx.doi.org/10.1016/j.cam.2004.07.008.
[18] J.A.C. Weideman, S.C. Reddy, A MATLAB differentiation matrix suite, ACM Trans. Math. Software 26 (4) (2000) 465–519. http://dx.doi.org/10.1145/365723.365727.
[19] P. Amodio, F. Iavernaro, Symmetric boundary value methods for second order initial and boundary value problems, Mediterr. J. Math. 3 (3–4) (2006) 383–398. http://dx.doi.org/10.1007/s00009-006-0085-7.
[20] Lloyd N. Trefethen, Spectral Methods in MatLab, Society for Industrial and Applied Mathematics, Philadelphia, PA, USA, 2000.
[21] M.J. Ablowitz, B.M. Herbst, C.M. Schober, On the numerical solution of the sine-Gordon equation. II. Performance of numerical schemes, J. Comput. Phys. 131 (2) (1997) 354–367. http://dx.doi.org/10.1006/jcph.1996.5606.
[22] S. Ober-Blöbaum, N. Saake, Construction and analysis of higher order Galerkin variational integrators, Adv. Comput. Math. 41 (6) (2015) 955–986. http://dx.doi.org/10.1007/s10444-014-9394-8.
[23] Myron S. Henry, John A. Roulier, Geometric convergence of chebyshev rational approximations on $[0, +\infty)$, J. Approx. Theory 21 (4) (1977) 361–374. http://dx.doi.org/10.1016/0021-9045(77)90007-7.
[24] D. Gaier, Polynomial approximation of piecewise analytic functions, J. Anal. (4) (1996) 67–79.
[25] S.M. Cox, P.C. Matthews, Exponential time differencing for stiff systems, J. Comput. Phys. 176 (2) (2002) 430–455. http://dx.doi.org/10.1006/jcph.2002.6995.
[26] Aly-Khan Kassam, Lloyd N. Trefethen, Fourth-order time-stepping for stiff pdes, SIAM J. Sci. Comput. 26 (4) (2005) 1214–1233. http://dx.doi.org/10.1137/S1064827502410633.
[27] A.Q.M. Khaliq, J. Martín-Vaquero, B.A. Wade, M. Yousuf, Smoothing schemes for reaction–diffusion systems with nonsmooth data, J. Comput. Appl. Math. 223 (1) (2009) 374–386. http://dx.doi.org/10.1016/j.cam.2008.01.017.
[28] Nicholas J. Higham, The scaling and squaring method for the matrix exponential revisited, SIAM J. Matrix Anal. Appl. 26 (4) (2005) 1179–1193. http://dx.doi.org/10.1137/04061101X.
[29] Marlis Hochbruck, Christian Lubich, Hubert Selhofer, Exponential integrators for large systems of differential equations, SIAM J. Sci. Comput. 19 (5) (1998) 1552–1574. http://dx.doi.org/10.1137/S1064827595295337.
[30] Jitse Niesen, Will M. Wright, Algorithm 919: A krylov subspace algorithm for evaluating the ϕ-functions appearing in exponential integrators, ACM Trans. Math. Software 38 (3) (2012) 22:1–22:19. http://dx.doi.org/10.1145/2168773.2168781.